Liu and He
EURASIP Journal on Advances in Signal Processing (2024) 2024:68
https://doi.org/10.1186/s13634-024-01154-y

EURASIP Journal on Advances in Signal Processing

RESEARCH Open Access

Design and analysis of CP-free OFDM PDMA transmission system

Jiao Liu[1,2*] and Jianqiang He[1,2]

*Correspondence:
230043@slxy.edu.cn

[1] Electronic Information and Electrical College of Engineering, Shangluo University, Shangluo 726000, Shaanxi, China
[2] Shangluo Artificial Intelligence Research Center, Shangluo 726000, China

Abstract

The paragraph introduces a proposed CP-free OFDM PDMA downlink transmission system. The main focus of the system is to address the capacity limitations caused by the overhead of cyclic prefix in traditional PDMA systems. The transmitter utilizes a pattern mapping unit before CP-free OFDM modulation to enhance system capacity and frequency efficiency. Decision feedback equalization (DFE) is employed in the receiver to eliminate intersymbol interference. The output signals from the DFE are then passed through a CP restoration unit to convert a linear-shifted signal into a cyclic-shifted signals. To assess the system's performance, simulations are conducted, investigating different key parameters such as overload rate, channel condition, and signal-to-noise ratio. The results indicate that, compared to CP OFDM PDMA systems, the proposed CP-free PDMA system significantly enhances system capacity under the same overload rate. Additionally, bit error rate is also evaluated during the simulations. Overall, the paragraph provides an overview of the proposed CP-free OFDM PDMA system, its components, and the simulation-based evaluation of its performance compared to traditional PDMA systems.

Keywords: PDMA, OFDM, Cyclic prefix, DFE, Bit error rate

1 Introduction

The surge in the number of access terminals in mobile communication networks, driven by the development of social intelligence, has created a pressing challenge in utilizing limited wireless resources to accommodate more terminals and enhance system throughput in mobile communications. Non-orthogonal multiple access (NOMA) has been investigated as a potential solution for upcoming networks like beyond 5G and 6G networks. The advantages of NOMA are recognized for meeting the performance requirements of 6G networks, particularly in terms of extensive connectivity [1, 2]. NOMA is a technique for multiple access that enables simultaneous sharing of frequency and temporal resources among users [3]. It accomplishes this through power domain multiplexing, where users are allocated different power levels based on their individual channel conditions. As a result, users with weaker signal strengths can utilize the shared resources alongside users with stronger signals simultaneously. PDMA represents a new form of NOMA technology, founded on the comprehensive optimization of multi-user communication systems as proposed following

Springer Open

© The Author(s) 2024. **Open Access** This article is licensed under a Creative Commons Attribution 4.0 International License, which permits use, sharing, adaptation, distribution and reproduction in any medium or format, as long as you give appropriate credit to the original author(s) and the source, provide a link to the Creative Commons licence, and indicate if changes were made. The images or other third party material in this article are included in the article's Creative Commons licence, unless indicated otherwise in a credit line to the material. If material is not included in the article's Creative Commons licence and your intended use is not permitted by statutory regulation or exceeds the permitted use, you will need to obtain permission directly from the copyright holder. To view a copy of this licence, visit http://creativecommons.org/licenses/by/4.0/.

early SAMA technology research. PADM leverages PDMA patterns to segregate user signals at the transmitter, enabling their realization across multiple resource domains [4, 5]. For multi-user detection, the terminal employs the generalized successive interference cancelation (SIC) detection algorithm [6]. Recent investigations have explored more sophisticated receivers for PDMA. In [7], an iterative detection and decoding algorithm is proposed, while [8] introduces a joint PDMA receiver algorithm that integrates the SIC detection algorithm with the minimum mean square error (MMSE) detection algorithm and associates cyclic redundancy check (CRC) to mitigate error propagation in the SIC receiver [9]. The allocation of PDMA overload to physical resources is elucidated through a pattern matrix. The principles and procedures of the PDMA pattern matrix are expounded in [10], which delineates diverse pattern design criteria tailored to distinct 5G uplink service requisites. The value of the PDMA pattern matrix hinges on the trade-off between the desired multiplexing factor and the system implementation complexity [11]. Additionally, it is generally observed that the multi-user pattern design methods vary based on the characteristics of different signal domains. Notably, for a PDMA system overloading J users on K sub-carriers, its pattern matrix is denoted as

$$\mathbf{P}^{[K,J]} = [\mathbf{p}_1, \mathbf{p}_2, \cdots, \mathbf{p}_J] \tag{1}$$

where $\boldsymbol{p}_j$ ($j \in \{1,2,\ldots, J\}$) is a K-dimensional column vector representing the pattern vector of user j.

For example, a pattern matrix with four sub-carriers and six users can be expressed as

$$P^{[4,6]} = \begin{bmatrix} 111100 \\ 110100 \\ 111010 \\ 100001 \end{bmatrix} \tag{2}$$

where j-th column of the pattern matrix P represents the pattern vector of user j, and the k-th row indicates the overloaded user situation on the k-th sub-carrier.

In PDMA pattern design, a combination of PDMA and multiple-input multiple-output (MIMO) was proposed in [12]. The paper also presents a receiver detection algorithm for the MIMO–PDMA scheme and analyzes the performance of MIMO–PDMA in both power and code domains. In [13], various PDMA multi-user power allocation methods are discussed, including global search power allocation, fixed power allocation, and partial power allocation. However, the specific implementation process and performance analysis of these methods were not provided. To optimize the throughput of all users, a scheme of joint pattern allocation and power allocation based on the water-filling algorithm was proposed in [14]. One of the advantages of PDMA technology is its ability to design non-orthogonal feature patterns using multi-dimensional domains. This allows for a wider application range and high flexibility, as there is no restriction on the number of users sharing the same resource. PDMA can fully utilize the benefits of multi-dimensional domain processing.

Orthogonal frequency division multiplexing (OFDM) technology originated in the mid-1950s. In an OFDM system, a high-rate data stream is divided into several lower-rate sub-streams. The data information is then carried by a set of orthogonal sub-carriers after undergoing an inverse fast Fourier transform (IFFT). OFDM is widely used in various wireless systems due to its ability to effectively handle the delay spread of wireless channels [15]. To completely mitigate intersymbol interference (ISI) in OFDM systems, an adequate cyclic prefix (CP) must be inserted at the beginning of every OFDM block before transmission. At the receiver, demodulation of the original OFDM symbol is successful upon removal of the CP. However, the use of CP introduces additional bandwidth consumption, leading to a loss in spectral efficiency, energy efficiency, and transmission rate. This issue becomes more critical in scenarios with long-delay extension, where the CP overhead becomes significant and reduces the spectral efficiency of OFDM systems. Addressing this challenge, a CP-free OFDM transmission scheme is proposed in [16]. This scheme incorporates decision feedback equalization (DEF) and CP restoration units, utilizing a symbol cyclic-shift equalization algorithm to eliminate both ISI and inter-carrier interference (ICI). [17] proposes a minimum mean square error iterative receiver based on parallel interference cancelation for CP-free OFDM signal reception. Moreover, an AI-aided CP-free OFDM system, utilizing artificial intelligence methods for channel estimation and signal detection, is investigated in [18]. The impact of removing CP in massive multiple-input multiple-output (MIMO) OFDM systems is discussed in [19–21]. In [22], a CP-free OFDM signal detection method is realized in the receiver. However, it is important to note that this method may sacrifice real-time performance of signal processing. [23] proposes DNN-based estimation in offline training and detection in online testing of downlink power domain multi-user NOMA-OFDM symbols robust against various channel impairments.

In this article, we propose a CP-free orthogonal frequency division multiplexing (OFDM) pulse division multiple access (PDMA) downlink system. The transmitter consists of PDMA encoding and CP-free OFDM modulation. The receiver includes CP restoration, OFDM demodulation, decision feedback equalizer (DFE), and PDMA multi-user detection. DFE is a commonly used method to eliminate intersymbol interference (ISI) in frequency-selective fading channels [24–26]. In [27], a sparse code division multiple access uplink access scheme based on time-domain precoding was proposed, which significantly improves system capacity by eliminating CP overhead. CP-free OFDM transmission allows for a reduction in bandwidth consumption, resulting in increased spectral efficiency. By combining CP-free OFDM with PDMA technology, the system's capacity can be further enhanced. PDMA enables multiple users to simultaneously access the downlink, thereby increasing the number of supported users and improving system capacity. The use of DFE in the receiver enhances the system's ability to recover the transmitted data accurately.

The rest of the paper is organized as follows. In Sect. 2, we introduce the system model and describe the signal processing procedure. In Sect. 3, we present the simulation results and evaluate the system's performance. Finally, in Sect. 4, we provide a conclusion.

2 System model

In this section, a block diagram of a CP-free OFDM PDMA system is presented.

2.1 CP-free OFDM PDMA transmitter

Figure 1 presents the block diagram of CP-free OFDM PDMA transmitter. In the transmitter, the data of the j-th user undergoes a series of operations, including channel encoding, constellation mapping, pattern mapping, parallel to serial conversion (P/S), and CP-free OFDM modulation. Let S_j denote the modulation symbol after constellation mapping, the PDMA pattern matrix $\hat{S}_j$ can be expressed as

$$\hat{\mathbf{S}}_j = S_j \cdot \mathbf{p}_j \tag{3}$$

where $\hat{\mathbf{S}}_j$ is a $K \times 1$ vector. In Fig. 1, the combiner linearly superimposes the signals of all J users, which are then send into a serial to parallel conversion (S/P) unit, followed by IFFT, P/S unit, and digital-to-analog conversion (DAC) unit before wireless transmission. The IFFT is performed on $\hat{\mathbf{S}}_j$ to generate an OFDM signal $\tilde{\mathbf{S}}$, that is

$$\tilde{\mathbf{S}} = \mathbf{F} \sum_{j=1}^{J} \hat{\mathbf{S}}_j \tag{4}$$

where $\boldsymbol{F}$ is IFFT matrix. The only difference from a typical OFDM system, which usually inserts CP between adjacent OFDM blocks, is that CP-insertion is absent between OFDM blocks in order to maintain high spectral efficiency.

2.2 CP-free OFDM receiver

Figure 2 illustrates the primary structure of the CP-free OFDM PDMA receiver, which comprises the DFE, cyclic prefix recovery (CPR), and PDMA multi-user detection modules. Due to the presence of multipath, the signal suffers from intersymbol interference (ISI) and inter-carrier interference (ICI).

Here, we name $[\mathbf{R}_m(n)]_{n=0}^{K-1}$ as the Nyquist samples vector of the m-th OFDM symbol block in j-th user, it can be expressed as

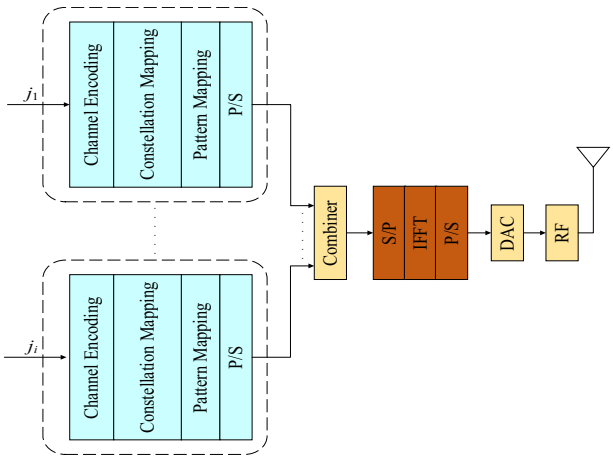

Fig. 1 The block diagram of CP-free OFDM PDMA transmitter

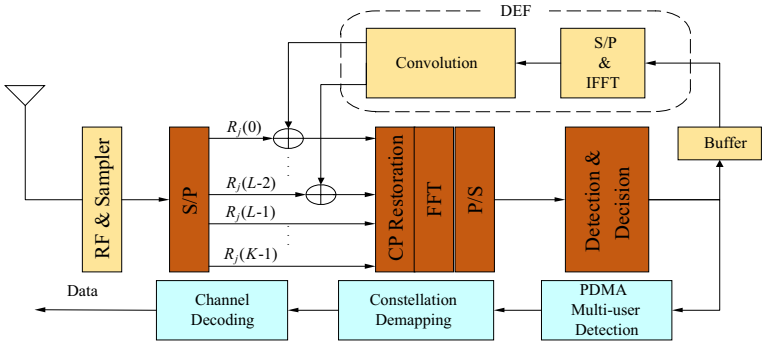

Fig. 2 The main structure of the CP-free OFDM PDMA receiver

$$
\begin{aligned}
[\mathbf{R}_m(n)]_{n=0}^{K-1} &= [\mathbf{R}_m(n)]_{n=0}^{L-2} + [\mathbf{R}_m(n)]_{n=L-1}^{K-1} \\
&= \left[\sum_{l=0}^{n} \rho_{j,l}\tilde{\mathbf{S}}_m(n-l)e^{i2\pi\varphi_{j,l}} + \mathbf{I}_m(n) + \mathbf{v}(n)\right]_{n=0}^{K-1} \\
&\quad + \left[\sum_{l=0}^{L-1} \rho_{j,l}\tilde{\mathbf{S}}_m(n-l)e^{i2\pi\varphi_{j,l}} + \mathbf{v}(n)\right]_{n=L-1}^{K-1}
\end{aligned} \tag{5}
$$

where ρ_{jl}denotes the channel attenuation of the l-th path of the j-th user, $2\pi\varphi_{j,l}$ is a multipath random phase that follows a uniform distribution over [0, 2π],$\tilde{\mathbf{S}}_m(n-l)$ is the (n-l)-th element of the m-th multi-user superposition time-domain vector transmitted by the base station, $\mathbf{I}_m(n)$is the tailing interference of the previous symbol when detecting the m-th symbol, and $\boldsymbol{v}(n)$ is the Gaussian noise on the n-th time-domain symbol.

Assuming that the channel state information is known, the previous samples are overlapped by the exceeding samples of the (m-1)-th symbol due to multipath propagation, with the length of the overlapping part being L-1. The reconstructed signal $C_{\text{m-1}}$ is obtained by convolving the (m-10)-th symbol $\tilde{\mathbf{S}}_{m-1}$ with the channel impulse response vector $\boldsymbol{h}_{\text{j}}$ as depicted in [16], resulting in Eq. (6).

$$
[\mathbf{C}_{m-1}(n)]_{n=0}^{K+L-2} = \left[\tilde{\mathbf{S}}_{m-1}(n)\right]_{n=0}^{K-1} * \left[\mathbf{h}_j(n)\right]_{n=0}^{L-1} \tag{6}
$$

Here, $[\mathbf{C}_{m-1}(n)]_{n=0}^{K+L-2}$ is a vector with $M+L$ -1 elements. Additionally, we assume the latter L-1 elements of the exceeding samples to be denoted as $[\mathbf{I}_m(n)]_{n=0}^{L-2}$, as expressed in Eq. (7).

$$
[\mathbf{I}_m(n)]_{n=0}^{L-2} = [\mathbf{C}_{m-1}(n)]_{n=K}^{K+L-2} \tag{7}
$$

Referring to Eq. (5), the acquisition of the interference component enables the elimination of intersymbol interference (ISI) by processing the interference term associated with the m-th symbol.

Furthermore, the symbol block is influenced by its inherent linear shift. To address this, the cyclic prefix recovery algorithm is employed to estimate and compensate for the trailing part of the m-th symbol, thereby bridging the initial gap. This process transforms the

linearly shifted signal into a cyclically shifted one. Subsequently, the original signal is reinstated through frequency domain equalization following a fast Fourier transform (FFT).

A challenge arises from the fact that the signal received encompasses a multipath superposition. In this context, a step estimation approach can be employed to determine the sampling values across all paths. Disregarding noise and the removal of the trailing part of the preceding symbol, the initial sampling value for the m-th symbol block is as Eq. (8).

$$\mathbf{R}_m(0) = \rho_0 e^{i2\pi\varphi_0}\tilde{\mathbf{S}}_m(0) \tag{8}$$

where ρ_0 and φ_0 represent the first channel attenuation and phase, respectively. The product of $\boldsymbol{R}_{\mathrm{m}}$ (0) and $\boldsymbol{h}_j/\boldsymbol{h}_j(0)$ is used to estimate the first sampling values of each path, i.e., $[\hat{\mathbf{R}}_{m,0}(0),\ \hat{\mathbf{R}}_{m,1}(0), \cdots, \hat{\mathbf{R}}_{m,L-1}(0)]$, where $\hat{\mathbf{R}}_{m,l}(0)$ represents the first sampling value on the m-th symbol block in path l. Obviously, the second sampling value is represented by $\boldsymbol{R}_m$ (1). The second sample value is interfered by the first sample value in the second path, where the latter has been estimated in the previous step. The estimated value of the second sampling value of the first path after eliminating the interference can be obtained by subtracting $\hat{\mathbf{R}}_{m,1}(0)$ from $\boldsymbol{R}_m$ (1), we can get

$$\hat{\mathbf{R}}_{m,0}(1) = \mathbf{R}_m(1) - \hat{\mathbf{R}}_{m,1}(0) \tag{9}$$

Then,$\hat{\mathbf{R}}_{m,0}(1)$ is multiplied by $\boldsymbol{h}_j$ / $\boldsymbol{h}_j$ (0) to estimate the second sample value of each path, *i.e.*, $[\hat{\mathbf{R}}_{m,0}(1),\ \hat{\mathbf{R}}_{m,1}(1), \cdots, \hat{\mathbf{R}}_{m,L-1}(1)]$. According to this inference, all K signal values of all paths can be estimated to complete CP reconstruction. Then, performed FFT gets

$$\mathbf{S}'_m(k) = \sum_{l=0}^{L-1}\left[\rho_{j,l}e^{-2\pi\left(\frac{kl}{K}-\varphi_{j,l}\right)}\right]\tilde{\mathbf{S}}_m(k) + \mathbf{v}'(k) + \varepsilon'_m(k) \tag{10a}$$

$$\mathbf{v}'(k) = \frac{1}{\sqrt{K}}\sum_{n=0}^{K-1}\mathbf{v}(n)e^{-i2\pi\frac{nk}{K}} \tag{10b}$$

$$\varepsilon'_m(k) = \frac{1}{\sqrt{K}}\sum_{n=0}^{K-1}\boldsymbol{\varepsilon}_m(n)e^{-i2\pi\frac{nk}{K}} \tag{10c}$$

where $\mathbf{v}'(k)$ is the Gaussian noise on the k-th sub-carrier, $\varepsilon'_m(k)$ is the decision feedback equalization error on the k-th sub-carrier, and $\boldsymbol{\varepsilon}_{\mathrm{m}}(n)$ is the decision feedback error on the n-th time-domain symbol.

2.3 Multi-user detection

The receiver employs the SIC algorithm for multi-user detection, which is organized according to the signal-to-interference-noise ratio (SINR). Initially, after resolving the signal for user 1, this signal is subtracted from the aggregated multi-user signal to mitigate the interference user 1 causes to others. This process is repeated sequentially until the signal of the last user is detected. For illustration, consider a PDMA system equipped with four sub-carriers ($K=4$) and six users ($J=6$). This example will elucidate the SIC process further.

The pattern matrix is delineated in Eq. (2). To enhance user discrimination and achieve superior multi-user detection performance, PDMA typically introduces a power factor to the basic pattern matrix as follows

$$\mathbf{G}^{[4,6]} = \begin{bmatrix} g_{1,1}g_{1,2}g_{1,3}\, g_{1,4}\, 00 \\ g_{2,1}\, g_{2,2}0g_{2,4}\, 00 \\ g_{3,1}g_{3,2}g_{3,3}0\, g_{3,5}0 \\ g_{4,1}000\, 0\, g_{4,6} \end{bmatrix} \tag{11}$$

The corresponding factor diagram is depicted in Fig. 3. Each row of $\boldsymbol{G}$ represents a carrier, and each column of $\boldsymbol{G}$ corresponds to a user. Consequently, the sum of the elements in a user's column in $\boldsymbol{G}$ indicates the transmit diversity order for that user. Similarly, the sum of the elements in a carrier's row in $\boldsymbol{G}$ indicates the overlap order for that carrier. The ratio of the number of columns to the number of rows represents the overload rate of the PDMA pattern.

The key of the proposed PDMA method lies in the pattern design, which can significantly affect both system performance and detection complexity. On the one hand, for a given K, different overload rates can support varying access connections. The larger the overload ratio, the better the system performance and the higher the detection complexity. On the other hand, for certain users, a higher transmit diversity order can achieve more reliable data transmission at the cost of more complex detection. Therefore, strategic pattern design is necessary to balance system performance and detection complexity.

As per the description above of the PDMA pattern, initially, the receiver performs detection priority sorting, which is based on the transmission diversity and average SINR of signals transmitted by each user. A higher transmission diversity yields more reliable transmission. If the transmission diversity is equal among users, their average SINR values are compared. For the 1st and 2nd users, the transmission diversities are 4 and 3, respectively, and are higher than those of subsequent users. So the 1st and 2nd users are detected preferentially. For the 3rd and 4th users, their transmission diversity values being equal,

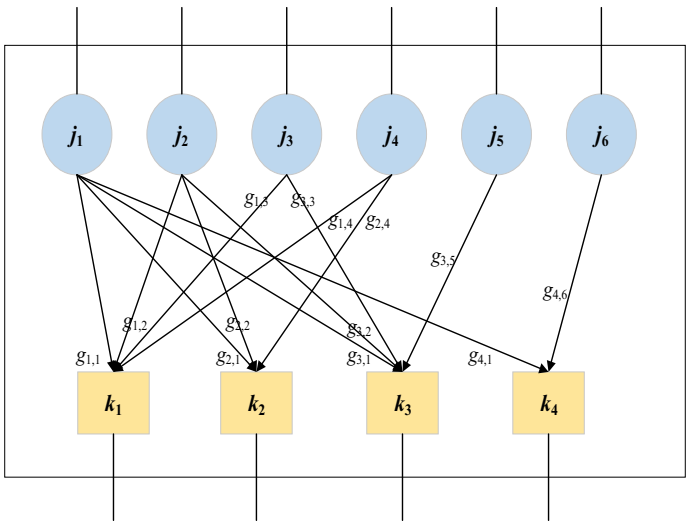

Fig. 3 The factor diagram of the PDMA pattern

a comparison of their average SINR values is undertaken. With the use of SIC detection, when detecting the 3rd and 4th users, it is assumed that the interference from the 1st and 2nd users is entirely eliminated. The 3rd user faces interference form from the 4th, 5th, and 6th users, while the 4th user's interference is from the 3rd, 4th, and 6th users. Consequently, the average SINR of the 3rd user can be expressed as

$$\overline{\gamma}_3 = \frac{\gamma_{1,3} + \gamma_{3,3}}{2} \tag{12a}$$

$$\gamma_{1,3} = \frac{g_{1,3}}{g_{1,4} + \sigma^2} \tag{12b}$$

$$\gamma_{3,3} = \frac{g_{3,3}}{g_{3,5} + \sigma^2} \tag{12c}$$

where $\gamma_{1,3}$ and $\gamma_{3,3}$ are the SINR of the 1st user on the 1st and 3rd sub-carriers, and σ^2 is the noise power. Similarly, the average SINR of the 4th user is calculated. By comparing their SINR, the one with the higher average SINR is detected first, using the maximum ratio combining method to amalgamate signals from different sub-carriers. Let $y_{k,j}$ denote the signals received by the j-th user on the k-th sub-carrier, the signal combined for decision-making is represented as follows

$$\hat{y}_j = \sum_{k=1}^{K} \lambda_{k,j} \cdot y_{k,j} \tag{13a}$$

$$\lambda_{k,j} = \frac{g_{k,j}}{(\sum_{n=j+1}^{J} g_{k,n} + \sigma^2)\psi_j} \tag{13b}$$

$$\psi_j = \sum_{k=1}^{K} \frac{g_{k,j}}{\sum_{n=j+1}^{J} g_{k,n} + \sigma^2} \tag{13c}$$

where ψ_j is the total SINR for the j-th user across all K sub-carriers, and if $g_{k,j}=0$, the SINR for the j-th user on the k sub-carrier equals zero and is not included in the total, $\lambda_{k,j}$ is the weight coefficient. $\lambda_{k,j}$ is actually the ratio of the SINR for the j-th user on the k sub-carrier to the total SINR across all K sub-carriers, as illustrated in Eqs. (13b, c). This definition confirms the optimality of the maximum ratio combination weight coefficient. After applying the maximum ratio combination to the signal of the j-th user, the signal form any undetected user is treated as noise in the decision process. The equivalent noise power received by the j-th user can be expressed as

$$\hat{\sigma}_j^2 = \sum_{k=1}^{K} \lambda_{k,j}^2 \cdot (\sum_{n=j+1}^{J} g_{k,n} + \sigma^2) \tag{14}$$

2.4 System capacity

The frequency domain response of the j-th user on the k-th sub-carrier is presented in Eq. (15).

$$\tilde{\mathbf{h}}_j(k) = \frac{1}{\sqrt{K}} \sum_{l=0}^{L-1} \rho_{j,l} e^{-i2\pi(\frac{kl}{K} - \varphi_{j,l})} \tag{15}$$

For the j-th user, the signal transmitted across different sub-carriers following pattern mapping results in a total capacity C_j, which equals the sum of the capacities of the signal on each sub-carrier as illustrated in [15], that can be expressed as

$$C_j = \sum_{k=1}^{K} C_{j,k} \tag{16a}$$

$$C_{j,k} = \frac{B}{K} \log_2(1 + \frac{P_s}{\sigma^2 + P_i}) \tag{16b}$$

$$P_s = g_{k,j} \left\| \tilde{\mathbf{h}}_j(k) \right\|^2 \tag{16c}$$

$$P_i = \left\| \tilde{\mathbf{h}}_j(k) \right\|^2 \sum_{n=j+1}^{J} g_{k,m} \tag{16d}$$

where B denotes the system bandwidth, B/K represents the bandwidth of a single sub-carrier, $C_{j,k}$ is the capacity of the j-th user on the k-th sub-carrier, P_s is the signal power of the signal from the j-th user on the k-th sub-carrier, P_i is the interference power from other users on the k-th sub-carrier, σ^2 is the noise power, and $||\cdot||$ is the modulus of the complex number.

The system's capacity, C, equals the sum of capacities of all users, as demonstrated in Eq. (17).

$$C = \sum_{j=1}^{J} \xi_j C_j \tag{17}$$

where ξj is the transmission efficiency. For CP-free OFDM systems, $\xi j = 1$, and for CP OFDM systems, $\xi j = K/(K + Lj - 1)$, where $(Lj - 1)$ is the maximum delay spread of the j-th user's channel, determined by $\boldsymbol{hj}$.

2.5 Complexity analysis

Compared with CP OFDM PDMA, the scheme we proposed achieves an improvement in capacity and performance at the expense of increased receiver complexity.

In the detection of the m-th multi-user superimposed symbol block, it is necessary to use the detected $(m-1)$-th symbol block that convolves with the channel response vector to reconstruct the tailing interference of the $(m-1)$-th symbol block. In this

process, the $(m-1)$-th symbol block also needs to undergo an IFFT to reconstruct the time-domain signal $\tilde{\mathbf{S}}_{m-1}$. The number of complex multiplications consumed in this process is $K/2\log_2 K$. In the convolution operation, the length of the input signal sequence is numerically equal to the number of sub-carriers K, and the length of the channel response vector is L. Therefore, the computational overhead of the convolution operation is $K \times L$. The total computational complexity generated by the DFE process is represented by Eq. (18).

$$O_{DEF} = K/2 \log_2 K + KL \tag{18}$$

The computational complexity in the process of CP reconstruction is mainly reflected in using the sample values of the first path signal to estimate the sample values of other paths, that is $[\mathbf{R}_m(n)]_{n=0}^{K-1} \cdot \frac{[h(0),h(1),\cdots,h(L-1)]}{h(0)}$, and then, the computational complexity generated by this process is represented by Eq. (19).

$$O_{CPR} = KL \tag{19}$$

The additional computational complexity of CP-free OFDM PDMA is the sum of the complexities of the DFE and CP reconstruction processes, denoted as $O_{DEF} + O_{CPR}$.

3 Simulation results and discussions

This section presents simulated results. Unless otherwise specified in the simulation, the number of sub-carriers K is set to 16, the number of users per carrier is J, and the overload rate is defined as $\eta = J/K$. The modulation scheme employed is quadrature phase shift keying (QPSK), and the total bandwidth is set to 1 MHz. The CP length is set equal to the maximum channel delay spread for a traditional CP OFDM system. The channel models used in the simulation include the extended typical urban channel model (ETU) and the extended vehicle channel model (EVA) channel models.

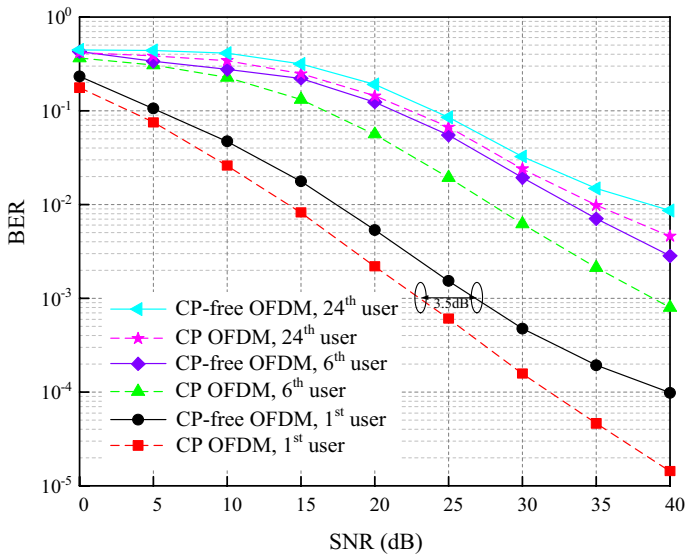

Fig. 4 BER performance of CP-free OFDM PDMA system and CP OFDM PDMA system in ETU channel model with overload rate $\eta = 150\%$

Figure 4 illustrates the simulation results of BER comparison between the CP-free OFDM PDMA system and the CP OFDM PDMA system for the 1st, 6th and 24th users when the overload rate in an ETU environment is 150%. From Fig. 4, it is evident that the BER performance improves as the SNR increases. However, the overall BER of the CP-free OFDM PDMA system is marginally higher than that of the CP OFDM PDMA system. For instance, considering the 1st user, to achieve a comparable BER performance of 10^{-3} with the CP OFDM PDMA system, the CP-free OFDM PDMA system exhibits a 3.5 dB loss in signal-to-noise ratio (SNR) performance. This loss can be attributed to two main factors. Firstly, as analyzed in Sect. 2, CP reconstruction introduces significant additional noise to the CP-free OFDM system, leading to decision feedback errors at the receiver. Secondly, the BER performance of users progressively worsens with the increase in the demodulation order. This deterioration is caused by the error propagation effect of SIC.

To investigate the impact of the overload rate η on the BER performance, simulations were conducted as illustrated in Fig. 5. These simulations compared the BER performance of the 6th user under CP-free OFDM PDMA and CP OFDM PDMA across different overload rates in ETU scenarios. Figure 5 demonstrates that the overload rate η significantly affects the system's BER performance. At an overload rate of $\eta = 100\%$, where one user's date is transmitted on one sub-carrier, the multi-user interference is minimal, and the BER performance is optimal. As the overload rate η increases, so does the multi-user interference. When the BER reaches 10^{-2}, the CP-free OFDM PDMA system with $\eta = 150\%$ experiences a 17 dB loss in SNR performance when compared to the CP-free OFDM PDMA system with $\eta = 100\%$. At an overload rate of $\eta = 200\%$, BER curve of the 6th user has shown a deterioration layer, and the main factor affecting the system's BER performance shifts from noise to the interference from other users.

Figure 6 provides a comparative assessment of the BER performance of a cyclic prefix CP-free OFDM PDMA system operating in an ETU channel environment, contrasted

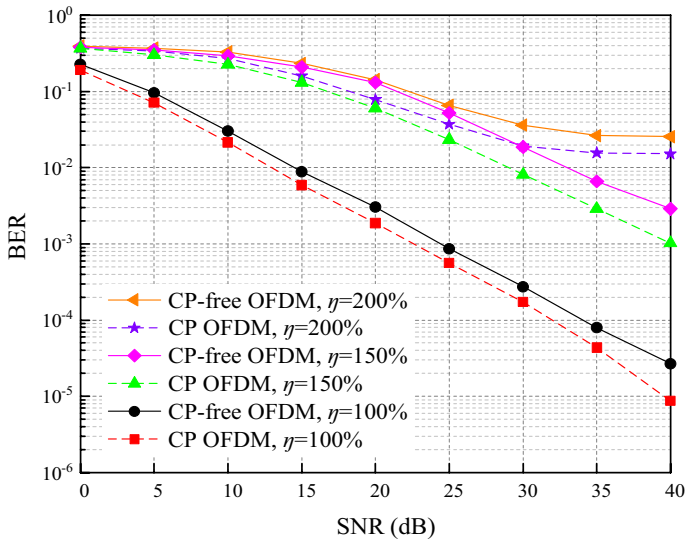

Fig. 5 BER performance of the 6th user under CP-free OFDM PDMA system and CP OFDM PDMA system with different overload rates in ETU channel model

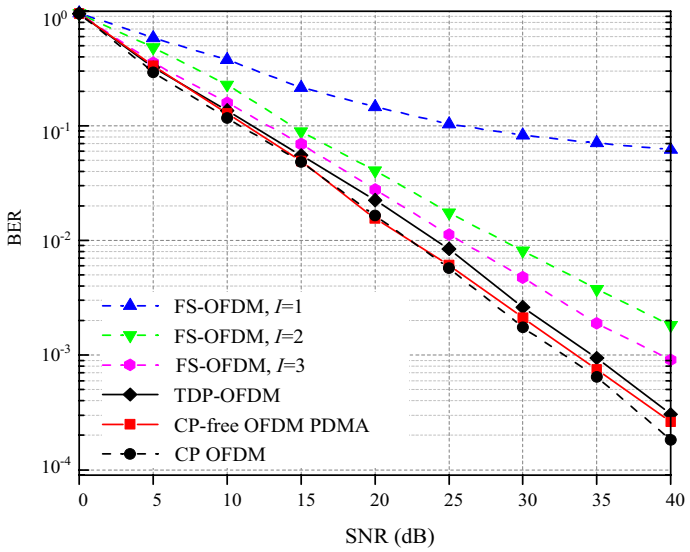

Fig. 6 BER performance of CP-free OFDM PDMA, TDP-OFDM, FS-OFDM, and CP OFDM system in ETU channel model

against the time-domain precoding (TDP) OFDM technique described in [28] and the feature suppressed OFDM (FS-OFDM) algorithm presented in [29]. FS-OFDM, recognized as a CP-free OFDM transmission strategy predicated on iterative interference suppression, involves iteratively reconstructing the CP until a stable BER performance level is achieved. It is important to note that, while the reconstructed CP serves as an approximation of the authentic CP, it is incapable of completely eliminating ICI. In Fig. 6, the symbol *'I'* denotes the iteration count for FS-OFDM, demonstrating a progressive improvement in its BER performance as the number of iterations increases, this iterative reception strategy compromises the real-time processing capabilities of signal processing. In contrast, TDP-OFDM avoids the use of the conventional CP by dividing a lengthy OFDM symbol into numerous sub-symbols, interspersing these with protective intervals to substitute the conventional CP structure. This approach simultaneously preserves the intrinsic resilience of OFDM to frequency-selective fading while circumventing the bandwidth loss associated with CPs. In environments characterized by pronounced multipath effects, such as the ETU channel, TDP-OFDM exhibits a relatively strong BER performance. Nonetheless, it is inherently reliant on the accuracy and update frequency of the channel state information (CSI), inaccuracies in CSI may potentially compromise the BER. The CP-free OFDM PDMA system leverages pattern division to establish user orthogonality, thereby significantly enhancing both spectral efficiency and system capacity. Additionally, under multipath conditions, its BER performance closely resembles that of a CP OFDM system.

The SNR and overload factor fluctuation curves for the CP-free OFDM PDMA system and the CP OFDM PDMA system in the ETU channel model are depicted in Fig. 7. As observed in Fig. 7, for an equivalent overload factor, the CP-free OFDM PDMA system exhibits a higher system capacity than the CP OFDM PDMA system, attributable to the elimination of the CP cost. When the capacity is 1.6×107 and $\eta = 250\%$, the CP OFDM PDMA system requires a 17 dB lower SNR compared to the

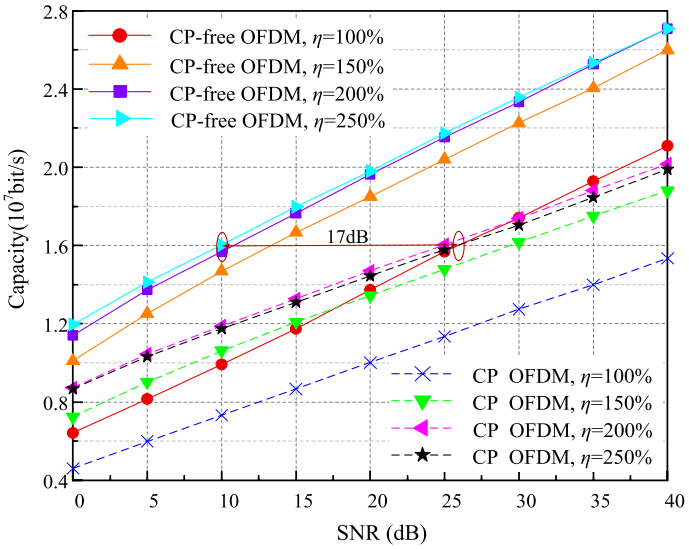

Fig. 7 Capacity of CP-free OFDM PDMA and CP OFDM PDMA system with different overload factor in ETU channel model

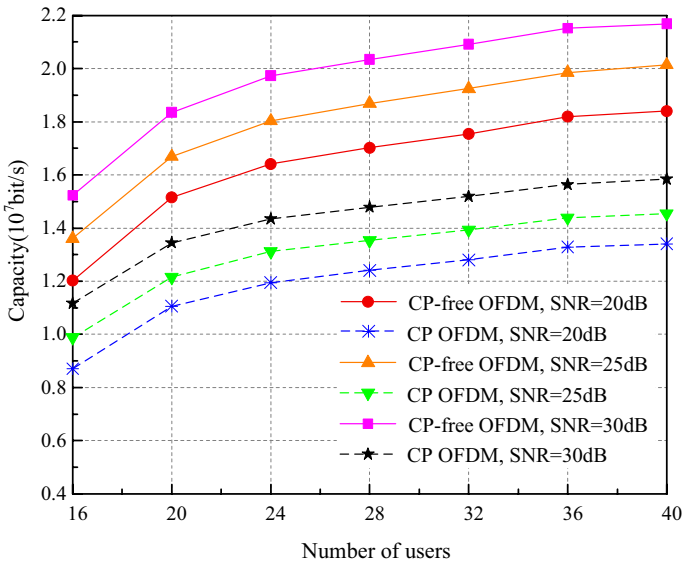

Fig. 8 Capacity of CP-free OFDM PDMA and CP OFDM PDMA system under different numbers of users in ETU channel model

CP OFDM PDMA system. Furthermore, at lower overload rates, the system capacity incrementally increases with rising overload rates. However, at higher overload rates, the escalation of multi-user interference becomes a significant hindrance, thus impeding further increases in system capacity.

Figure 8 exhibits the fluctuation curve representing system capacity as a function of user count under varying SNR for CP-free OFDM PDMA and CP OFDM PDMA in channel model. It can be discerned from the diagram that, in the scenario of a limited user base, system capacity experiences an incremental elevation with the

progressive increase in users. Yet, as user numbers further proliferate, the gradient of the system capacity curve verges on becoming negligible. This saturation point arises due to the intensification of multi-user interference as the user population augments, leading to a leveling off in capacity.

4 Conclusions

In this manuscript, we introduce a novel CP-free OFDM scheme for PDMA transmissions. This innovative approach significantly augments the system's capacity by eradicating the CP overhead, thereby enhancing spectral efficiency. Nonetheless, it is imperative to recognize that the PDMA system's capacity enhancement is constrained by the inherent multi-user interference, which inherently limits the scalability of system capacity with increase in system overload factors. Our simulations elucidate that beyond a 250% overload rate, there is a negligible increment in system capacity, indicating a plateau in capacity enhancement under high overload conditions. Furthermore, the adoption of CP-free OFDM technology, while is beneficial for capacity improvement, introduces reconstruction errors due to the CP elimination process. These errors slightly compromise BER performance of the PDMA system utilizing CP-free OFDM in comparison with its CP OFDM PDMA counterpart. However, this degradation in BER performance is deemed tolerable when juxtaposed with the notable gains in system capacity. In essence, this research underscores the CP-free OFDM PDMA system's superior capacity and bandwidth efficiency, establishing it as a formidable alternative to the traditional CP OFDM PDMA system. Through a comprehensive examination of the trade-offs between system capacity, BER performance, and spectral efficiency, this work contributes significantly to the ongoing discourse on optimizing transmission schemes for PDMA systems, highlighting the CP-free OFDM PDMA system's potential to redefine performance benchmarks in multi-user communication environments.

Acknowledgements
The authors would like to express their sincere thanks to the editors and anonymous reviewers.

Author contributions
JL designed the work, analyzed and interpreted the data, and drafted the manuscript. JQH participated in the design of the study, performed the experiments and analysis, and helped to draft the manuscript. Both authors critically revised, read, and approved the final manuscript.

Funding
This work was supported in part by the National Natural Science Foundation of China under Grant 11847042, Shangluo City Science and Technology Development Plan Project under Grant 2023-G-0029, Shangluo University Science and Technology Innovation Team Project under Grant 18SCX004.

Availability of data and materials
The datasets generated or analyzed during the current study are available from the corresponding author on reasonable request.

Declarations

Ethics approval and consent to participate
Not applicable.
Consent for publication
All authors of this paper agreed to publish the work in this paper.

Competing interests
The authors declare that they have no competing interests.

Received: 27 December 2023 Accepted: 15 April 2024
Published online: 03 June 2024

References

1. W.U. Khan, F. Jameel, M.A. Jamshed et al., Efficient power allocation for NOMA-enabled IoT networks in 6G era. Phys. Commun. **39**, 101043 (2020)
2. Y. Liu, W. Yi, Z. Ding et al., Developing NOMA to next generation multiple access: future vision and research opportunities. IEEE Wirel. Commun.Wirel. Commun. **29**, 120–127 (2022)
3. B. Makki, K. Chitti, A. Behravan et al., A survey of NOMA: current status and open research challenges. IEEE Open J. Commun. Soc. **99**, 179–189 (2020)
4. X. Dai, S. Chen, S. Sun, Successive interference cancelation amenable multiple access (SAMA) for future wireless communications. IEEE ICCS (2014).
5. S.Z. Chen, B. Ren, Q.B. Gao, Pattern division multiple access-a novel nonorthogonal multiple access for fifth-generation radio network. IEEE Trans. Veh. Technol. **66**(4), 3185–3196 (2017)
6. W. Tang, S. Kang, B. Ren, Uplink grant- free pattern division multiple access (GF-PDMA) for 5G radio access. China Commun. **14**(4), 153–163 (2018)
7. B. Ren, X. Yue, W. Tang, advanced IDD receiver for PDMA uplink system. IEEE ICCC (2016).
8. D. Kong, J. Zeng, X. Su, Multiuser detection algorithm for PDMA uplink system based on SIC and MMSE. IEEE ICCC (2016).
9. R. R. Singh, V. N. Mohammed, M. Lakshmanan, Performance analysis of pattern division multiple access technique in SIC and PIC receiver. International Conference on Circuit, Power and Computing Technologies, IEEE (2017).
10. B. Ren, Y. Wang, X. Dai, Pattern matrix design of PDMA for 5G UL applications. China Commun. **13**(2), 159–173 (2017)
11. Y. Mao, J. Zeng, X. Su, Pattern design in joint space domain and power domain for novel multiple access. IEEE VTC Spring (2016).
12. W. Tang, S. Kang, J. Zhao, Design of MIMO-PDMA in 5G mobile communication system. IET Commun. **14**(1), 76–83 (2020)
13. J. Zeng, B. Li, X. Su, Pattern division multiple access (PDMA) for cellular future.radio access. International Conference on Wireless Communications & Signal Processing (WCSP), IEEE(2015).
14. J. Zeng, B. Liu, X. Su, Joint pattern assignment and power allocation in PDMA, in *IEEE Vehicular Technology Conference, IEEE* (2017)
15. S. Weinstein, P. Ebert, Data transmission by frequency-division multiplexing using the discrete Fourier transform. IEEE Trans. Commun. Technol. **19**(5), 628–634 (1971)
16. X.Q. Liu, H. Chen, S.Y. Chen, Symbol cyclic-shift equalization algorithm: a CP-free OFDM/OFDMA system design. IEEE Trans. Veh. Technol. **66**(1), 282–294 (2017)
17. R. Bomfin, M. Chafii, G. Fettweis, A novel iterative receiver design for CP-Free transmission under frequency- selective channels. IEEE Commun. Lett. **24**(3), 525–529 (2020)
18. J. Zhang, C.K. Wen, S. Jin, Artificial intelligence-aided receiver for a CP-Free OFDM system:design, simulation, and experimental test. IEEE Access **7**, 58901–58914 (2019)
19. A. Farhang, A. Aminjavaheri, A. R. Reyhani, L. E. Doyle, B. Farhang-Boroujeny, Time reversal with post-equalization for OFDM without CP in massive MIMO, in *Symp. Wireless Commun. Syst. (ISWCS), Poznan, Poland*, pp. 352–358 (2016)
20. V. Nsengiyumva, Is the cyclic prefiifix needed in massive MIMO? M.S. thesis, Dept. Elect. Eng., Linkoping Univ., Linkoping, Sweden, 352–358(2016).
21. A. Aminjavaheri, A. Farhang, A. Rezazadehreyhani, L.E. Doyle, B. Farhang-Boroujeny, OFDM without CP in massive MIMO. IEEE Trans. Wirelss Commun. **16**(11), 7619–7633 (2017)
22. D. Kim, G.L. Stuber, Residual ISI cancellation for OFDM with applications to HDTV broadcasting. IEEE J. Sel. Areas Commun. **16**(8), 1590–1599 (1998)
23. A. Singh, S. Saha, Deep neural network based downlink power domain multi-user NOMA-OFDM signal detection. Eng. Res. Express **5**, 045008 (2023)
24. N. Benvenuto, S. Tomasin, Block iterative DFE for single carrier modulation. electron. lett. **38**(19), 1144–1145 (2002)
25. C. Belfifiore, J. Park, Decision feedback equalization. Proc. IEEE **67**(8), 1143–1156 (1979)
26. N. Benvenuto, S. Tomasin, On the comparison between OFDM and single carrier modulation with a DFE using a frequency-domain feedforward filter. IEEE Trans. Commun. **50**(6), 947–955 (2002)
27. L. Zhou, X.Q. Liu, Transceiver design and performance analysis for uplink SCMA based on CP-free OFDM. Telecommun. Sci. **37**(6), 23–32 (2021)
28. X.Q. Liu, H.H. Chen, X. Wang et al., Time domain precoding for OFDM/OFDMA systems without cyclic prefix. IEEE Trans. Veh. Technol.Veh. Technol. **67**, 5510–5514 (2018)
29. X.B. Wang, P. Ho, Y.Y. Wu, Robust channel estimation and ISI cancellation for OFDM systems with suppressed features. IEEE J. Sel. Areas Commun. **23**(5), 963–972 (2005)

Publisher's Note

Springer Nature remains neutral with regard to jurisdictional claims in published maps and institutional affiliations.